Available online at www.sciencedirect.com
ScienceDirect
Diamond & Related Materials 16 (2007) 718–724
DIAMOND AND RELATED MATERIALS
www.elsevier.com/locate/diamond

Surface composition, bonding, and morphology in the nucleation and growth of ultra-thin, high quality nanocrystalline diamond films

Anirudha V. Sumant [a,1], P.U.P.A. Gilbert [b,2], David S. Grierson [a], Andrew R. Konicek [b], Mike Abrecht [c], James E. Butler [d], Tatyana Feygelson [e], Shlomo S. Rotter [f], Robert W. Carpick [a,*,3]

[a] Department of Engineering Physics, University of Wisconsin-Madison, Wisconsin, 53706, United States
[b] Department of Physics, University of Wisconsin-Madison, Wisconsin, 53706, United States
[c] Synchrotron Radiation Center, University of Wisconsin, Stoughton, Wisconsin 53589, United States
[d] Gas/Surface Dynamics Division, Naval Research Laboratory, Washington, DC 20375, United States
[e] Science Applications International Corporation, Washington, DC 20003, United States
[f] Applied Diamonds, 1 Tet blvd. Rehovot 76100, Israel

Available online 31 January 2007

Abstract

The morphology, composition, and bonding character (carbon hybridization state) of continuous, ultra-thin (thickness ~60 nm) nanocrystalline diamond (NCD) membranes are reported. NCD films were deposited on a silicon substrate that was pretreated using an optimized, two-step seeding process. The surface after each of the two steps, the as-grown NCD topside and the NCD underside (revealed by etching away the silicon substrate) is examined by X-ray PhotoElectron Emission spectroMicroscopy (X-PEEM) combined with X-ray absorption near edge structure (XANES) spectroscopy, X-ray photoelectron spectroscopy (XPS), and atomic force microscopy (AFM). The first step in the seeding process, a short exposure to a hydrocarbon plasma, induces the formation of SiC at the diamond/Si interface along with a thin, uniform layer of hydrogenated, amorphous carbon on top. This amorphous carbon layer allows for a uniform, dense layer of nanodiamond seed particles to be spread over the substrate in the second step. This facilitates the growth of a homogeneous, continuous, smooth, and highly sp^3-bonded NCD film. We show for the first time that the underside of this film possesses atomic-scale smoothness (RMS roughness: 0.3 nm) and >98% diamond content, demonstrating the effectiveness of the two-step seeding method for diamond film nucleation.
© 2007 Elsevier B.V. All rights reserved.

Keywords: Nanocrystalline diamond; XANES; AFM; Nucleation

1. Introduction

The growth of conformal and continuous diamond films at nano-scale thicknesses (<100 nm) presents a scientific and technical challenge that is crucial for a range of applications including cold cathodes, flat-panel displays, atomic force microscopy (AFM) tips, wear-resistant coatings on micro-scale machine tools, and micro- and nano-electromechanical systems (MEMS/NEMS) devices, particularly RF switches and resonators for which mechanical and tribological properties must be optimized. The primary challenge is to enable growth on substrates, such as silicon, on which diamond does not naturally nucleate. Controlling the initial nucleation density via surface pretreatments is the key to obtain ultra-thin, continuous, highly sp^3-bonded diamond films on any substrate, including Si wafers. In a recent study, the nucleation density was shown to play a crucial role in improving the mechanical properties as well as the thermal diffusivity in ultra-thin nanocrystalline diamond (NCD) films [1]. Smoothness and compositional uniformity also significantly increase strength and resistance to fracture in nanocrystalline diamond films [2]. Additionally, the quality of the film–substrate interface depends on nucleation and plays a dominant role in reducing internal friction in NCD films, suggesting that a higher quality factor (Q) can be

* Corresponding author.
E-mail address: carpick@engr.wisc.edu (R.W. Carpick).
[1] Now at the Center for Nanoscale Materials, Argonne National Laboratory, Argonne, IL 60439, United States.
[2] Previously publishing as Gelsomina De Stasio.
[3] Now at the Department of Mechanical Engineering and Applied Mechanics, University of Pennsylvania, Philadelphia, PA 19104, United States.

0925-9635/$ - see front matter © 2007 Elsevier B.V. All rights reserved.
doi:10.1016/j.diamond.2006.12.011

obtained in NCD resonators when the film–substrate interface is tailored with an improved nucleation process [3].

The most widely used surface pretreatments involve modification of the substrate's surface either by abrading the surface with diamond particles [4] or bombarding the surface with diamond particles by immersing the substrate in a diamond suspension followed by ultrasonic agitation [5]. In the case of mechanical abrasion, micro- to nano-scale scratches or pits are produced on the surface, and these pits trap diamond fragments. The trapped fragments then act as nucleation seeds during subsequent diamond deposition. However, with ultrasonic agitation, diamond particles adhere to the surface due to van der Waal's interactions. These adhered diamond fragments then acts as nucleation seeds, which enables the growth of a uniform, continuous diamond film. Moderate nucleation densities ranging from 10^9 to 10^{11} nuclei/cm^2 have been reported using these methods. These are roughly seven orders of magnitude greater than that for a bare silicon surface, but still are not sufficient to obtain continuous films at nano-scale thicknesses. Abrading also causes considerable roughening of the substrate, resulting in diamond films that are not smooth, and this adversely affects the optical [6] and mechanical properties of the film. Bias-enhanced nucleation (BEN) [7] is another widely used method as it does not cause any mechanical damage to the substrate and provides a moderate nucleation density (10^{11} nuclei/cm^2) [8]. It is most effective on metallic and semiconducting substrates with the ability to form carbides since it involves implantation of carbon ions in the sub-surface region, creating a carbide-rich surface that enhances diamond nucleation [7]. This results in the precipitation of a predominantly non-diamond, carbon-rich layer at the interface which, according to a recent study, is likely to have poor tribological properties [9].

The process developed by S. Rotter [10] in 1999 and referred to in the literature as the "new nucleation process" (NNP) avoids problems mentioned above and provides nucleation densities in excess of 10^{12} nuclei/cm^2 for the growth of NCD films on silicon [1]. Recently, J. E. Butler et al. further modified NNP by making a small variation in the plasma treatment and subsequent seeding process [1,3]. Using this seeding process, they demonstrated the fabrication of resonator structures with a NCD film thickness as low as 80 nm [11].

The modified NNP process consists of two steps. The first step, referred to as the "plasma pretreatment" step, involves exposure of the substrate to the diamond growth environment in the deposition chamber for a short time period using the standard diamond growth parameters except for a higher methane concentration. In the second step, termed the "seeding" step, the Si substrate is taken out of the growth chamber and subjected to ultrasonic treatment in an alcohol solution with diamond nanopowder. The seeded substrate is then returned to the deposition chamber and diamond growth is initiated. This results in homogenous, smooth NCD films with the desired thickness, even as thin as 60 nm (thickness measured using AFM), as studied here.

Butler et al. have shown that the modified NNP process can be extended to other substrates and that the resultant NCD films have excellent mechanical and thermal properties with low internal friction [1,3]. However, the chemical nature of this process and the interfacial composition and structure of the resultant diamond films have not yet been investigated in detail. In this paper, we report the first comprehensive study of the morphology (via AFM), composition (via XPS), and bonding phase (via XANES/PEEM) for each stage of this nucleation process, for the film–substrate interface, and for the top surface of NCD film grown with this nucleation process.

2. Experimental

For the first step of the NNP process, a pre-cleaned Si wafer was loaded into the growth chamber and subjected to a plasma treatment for 30 min with the following process parameters: substrate temperature, 750 °C; microwave power, 800 W; chamber pressure, 15 Torr; H_2/CH_4 flow rate, 900/7 sccm. In the second step of the NNP process, the Si wafer was taken out of the growth chamber and then treated in an ultrasonic bath with either a methanol or ethanol solution containing diamond nanopowder (Plasmachem GMbH) [12] (mean grain size: 4–10 nm, synthesized using the detonation method) for 30 min followed by immediate rinsing in ethanol, and then blown dry with N_2. This is referred to as "seeding". The seeded wafer was then subjected to NCD growth in an AsTeX microwave plasma reactor (Model PDS-17, AsTeX Inc. Woburn, MA) operating at 2.45 GHz with a peak power of 1.5 kW using a H_2/CH_4 gas mixture with a minute amount (below 1 ppm) of unintentionally added boron. Growth was carried out for 30 min with essentially the same growth parameters used for the pretreatment step, except for a different gas ratio (H_2/CH_4: 900/3 sccm).

To conduct the experiments, the wafers were sectioned into ~1 cm^2 pieces and, when desired, immersed in a HF:HNO_3 (1:3) acid bath to dissolve the substrate to obtain free-standing NCD membranes. These were retrieved using a clean Si substrate, ensuring that the newly exposed underside now faced up. To hold this membrane in place, dots of silver paste were applied to its sides. Samples were then characterized using XPS, AFM, and X-PEEM spectromicroscopy. The AFM measurements were conducted in air with a Digital Instruments MultiMode AFM with a Nanoscope IV controller using intermittent contact mode. XPS measurements were conducted using a PHI-5400 ESCA system with a Mg anode for the X-ray source. X-PEEM was performed using the Spectromicroscope for the PHotoelectron Imaging of Nanostructures with X-rays (SPHINX) instrument [13] at the Synchrotron Radiation Center (SRC), University of Wisconsin-Madison. Simultaneous imaging and electron yield XANES spectra can be acquired with high lateral spatial resolution (down to 10 nm in the ideal case) [14] and a sensitivity depth of ~5 nm. All spectra were first normalized by ratio to a reference spectrum simultaneously taken on a separate region of the sample that was coated with high purity platinum. Subsequently, the intensity was also normalized to set the pre- and post-edge regions of the spectrum to zero and one, respectively. The normalization to the platinum reference eliminates the effects of absorption in the beamline due to carbon contamination, while setting the post-edge intensity to one allows the relative peak intensities within each spectrum to be compared.

3. Results and discussion

The evolution of the substrate's surface after both the plasma pretreatment and the seeding steps was analyzed. Additionally, to understand the bonding nature on the topside (growth side) and underside (nucleation side), both sides of the released NCD membranes were also studied.

Fig. 1 shows XPS C1s and Si2p core level spectra of the Si substrate after the plasma pretreatment (plots (a1) and (b1) respectively) and after seeding with diamond nanopowder (plots (a2) and (b2) respectively). Well-defined peaks at 282.6 eV and 100.2 eV are observed in C1s and Si2p core level spectra, which are assigned to the covalent Si–C bond. The formation a SiC phase during the early phases of diamond deposition has been observed previously [8,15,16] and sensitively depends on the substrate temperature and methane-to-hydrogen ratio [17]. Given the substrate temperature (750–800 °C) and the high methane ratio during the plasma pretreatment step, the formation of SiC is consistent with these previous experiments. The other peaks in the C1s high-resolution spectrum at 284.4 eV and 286.4 eV are assigned to amorphous carbon (C–C) and oxygenated carbon (C–O) respectively. In the Si2p high-resolution spectrum, the peaks at 98.8 eV and 102.3 eV are assigned to the elemental Si and the native oxide on the Si substrate. The presence of a small amount of native oxide detected in the XPS is may be due to the fact that the substrate was exposed to air after the treatment. The C and Si atomic concentrations are 32.6% and 38.6% respectively. The remainder is due to oxygen.

The C–C peak intensity increased significantly (atomic concentration: 62%) after seeding with nanodiamond powder, as expected (Fig. 1, a2). The C–Si peak decreased correspondingly. The intensity of the Si2p peak is also reduced (atomic concentration: 14.4%) (Fig. 1, b2) since the substrate is now covered with a layer of nanodiamond powder. Interestingly, the C–O peak area increased after the seeding process (Fig. 1, a2) and the C–C peak is shifted to a higher binding energy by 0.5 eV. Nanodiamond powder used here for seeding is synthesized using a detonation method and is known to contain metal impurities. Acid etching is often used to remove the metal impurities, but it results in oxidation of the nanodiamond [12]. The known presence of oxygenated species in detonation-synthesized nanodiamond and in other conjugated organic molecules is sufficient to explain the observed increase in the binding energy of the C–C peak [18,19].

To obtain further insight into the nature of carbon bonding and microstructural changes during the nucleation process, samples from the same wafer at each nucleation stage are subjected to AFM and XANES characterization. Fig. 2(a–c) shows XANES spectra and corresponding AFM images from the silicon substrate after the first (plasma pretreatment) and second (nanodiamond powder deposition) steps of the seeding process. X-ray absorption due to the presence of carbon is observed after the first step (Fig. 2a, spectrum b) and is distinct from that observed on Si substrates with adventitious carbon present [20]. Note that the thickness of the film deposited by the plasma pretreatment process is estimated to

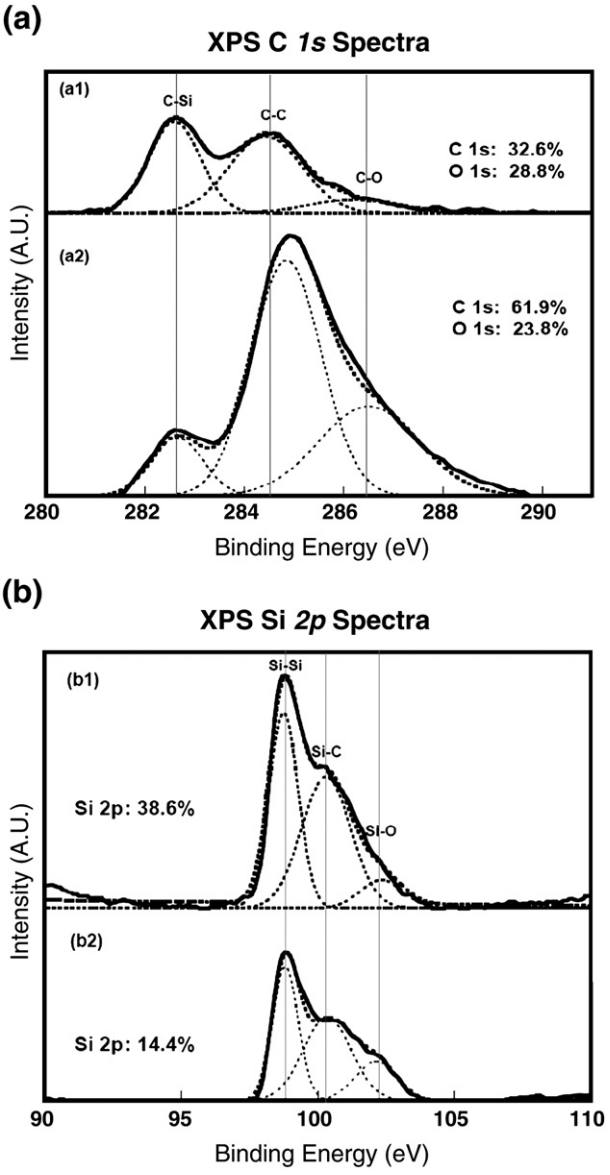

Fig. 1. XPS spectra of Si substrate at C1s (a) and Si2p (b) edges, respectively, indicating the formation of a SiC phase.

be less than 6 nm based on earlier TEM studies [21] and this may explain why only a weak XANES signal is observed. The spectrum shows a strong peak at 285.5 eV, which is due to the C1s→π* transition, and is characteristic of sp^2-bonded carbon such as that found in graphite or amorphous carbon [22]. This transition is normally observed at 285.0 eV for amorphous carbon [23]. The slight upshift in the C1s→π* peak may be due to the presence of Si–C [20] or graphite [22] at the interface. Additionally, there is a small, broad dip in the spectrum from ~298 to 300 eV, which is a characteristic feature observed in SiC XANES spectra [20]. The shoulder at 287.5 eV is due to C–H bonds [22]. This is expected in the amorphous carbon layer due to the hydrogen-rich gas chemistry of the plasma pretreatment process. The broad peak above 290 eV is associated with the σ-bonds found in amorphous carbon. Overall, the spectrum is distinct

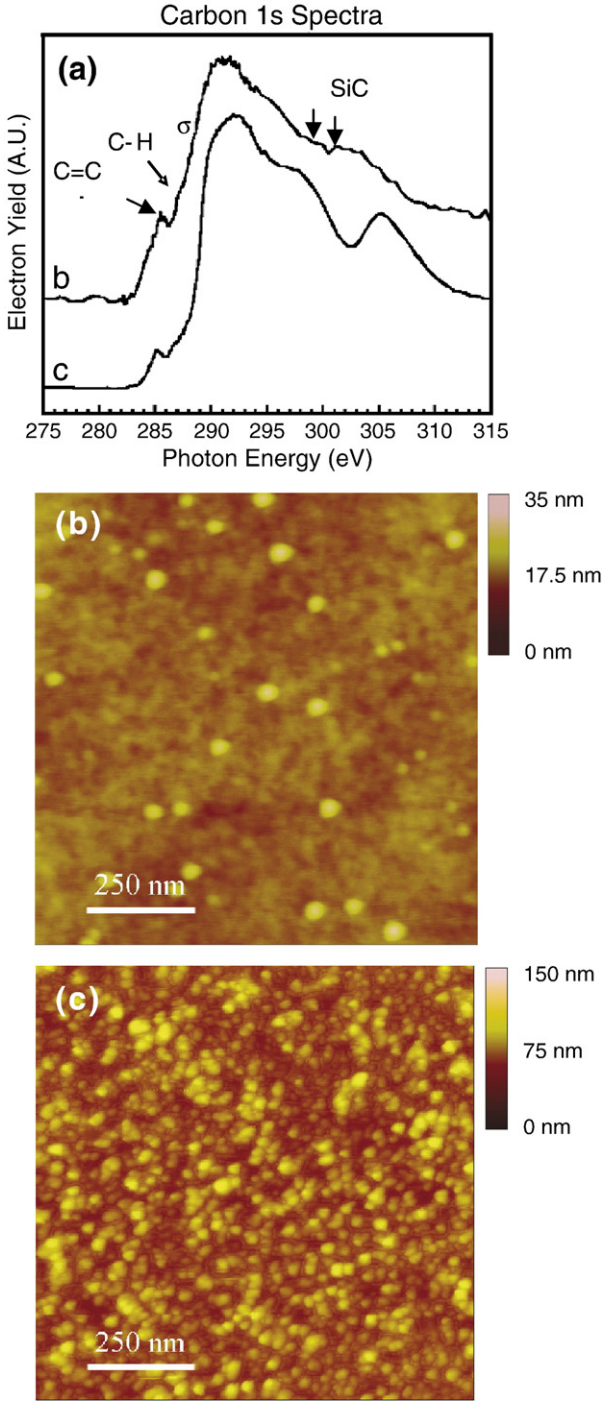

Fig. 2. (a) XANES spectrum of the sample after plasma treatment (spectrum b) and after seeding with nanodiamond powder (spectrum c). (b) and (c) are intermittent contact mode AFM topographic images of the corresponding samples. The high density of nanopowder distributed on the surface in (c) is clearly seen.

from that observed for typical hydrogenated diamond like carbon (DLC) films, which exhibit a larger C1s→π* peak at 285 eV, and a broader feature at 290 eV [24], indicating a lower percentage of sp^2-bonded carbon in this plasma pretreated layer. This spectrum therefore clearly demonstrates that the plasma pretreatment forms SiC at the interface along with a layer of amorphous carbon that is rich in hydrogenated, sp^3-bonded carbon.

The AFM topographic image (Fig. 2(b)) of the sample exposed to the plasma pretreatment shows a randomly rough surface with 1.36 nm RMS roughness (over the 1×1 μm^2 area) and round nano-scale particles (diameter: 37–56 nm, height: 4–11 nm) distributed randomly on the surface. These could be diamond nuclei formed during the pretreatment, amorphous agglomerates formed during the plasma exposure, or other contaminants. The density and size of these nano-scale particles are too small to be detected in the X-PEEM.

The spectrum acquired on the Si substrate after seeding with the diamond nanopowder (Fig. 2(a), spectrum c) is significantly different. The peak at 285 eV is smaller than before, indicating a lower fraction of sp^2-bonded carbon being sampled. The edge at ~290 eV is steeper, consistent with a higher fraction of sp^3-bonded carbon. A dip at 302.4 eV is evident, and this feature is associated with the second band-gap seen in crystalline diamond [25,26]. These spectral features clearly demonstrate that the majority of the signal comes from the diamond nanopowder. This indicates that the powder is distributed densely on the plasma pretreated Si substrate. The absence of a well-defined diamond exciton (expected at 289.3 eV) could be due to the small grain size of the nanodiamond powder, consistent with earlier observations [27]. The AFM topographic image (Fig. 2(a), spectrum c) shows uniformly, densely distributed nano-scale (diameter: 20–35 nm) particles on the substrate. From the XANES spectrum we can conclude that these features are the diamond nanoparticles. Therefore, the plasma pretreatment creates a surface on which the diamond nanopowder particles densely and uniformly distribute themselves.

Peak identification and height analysis of the AFM images were performed using a custom software code [28]. These measurements yielded average peak densities on the order of 1.3×10^{11} nanoparticles/cm^2. This is a lower bound for the nucleation density for diamond growth, since multiple nucleation sites can occur on a single particle, and the AFM image may not identify every single particle due to limited lateral spatial resolution.

Explosively formed nanodiamonds have been shown to have individual grains in the size range of 3 to 5 nm by TEM. When solutions of the nanodiamonds are made, the individual particles are generally agglomerated into much larger particles, 30 nm in size and larger. It is likely that the AFM is detecting agglomerates of nanodiamonds. During diamond growth, the high atomic hydrogen flux of the growth environment can break up agglomerates of nanodiamonds into smaller particles due to the etching effect of atomic hydrogen. Diamond nucleation then proceeds on these smaller diamond nuclei.

We propose that neither the SiC nor the amorphous carbon formed during pretreatment takes direct part in diamond nucleation, as that occurs directly on the topmost nanodiamond seed layer. However, formation of SiC at the interface may act as a diffusion barrier during carbon deposition. If so,

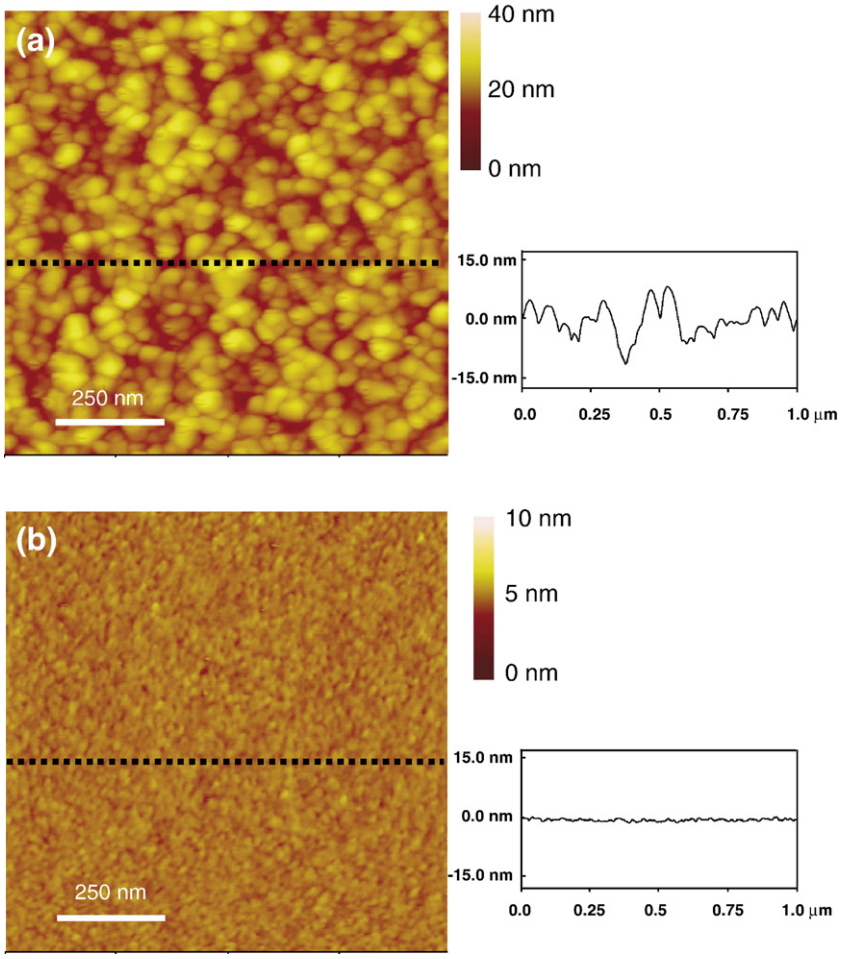

Fig. 3. AFM topographic images of the top side (a) and underside (b) of the 60 nm-thick NCD film, with corresponding cross sections from the lines indicated in the images.

the initial incubation time for nucleation will be substantially reduced, as almost all of the carbon flux will be utilized in forming diamond nuclei.

Figs. 3(a, b) show 1×1 μm^2 AFM topographic images of the top and undersides of the 60 nm-thick NCD film respectively, which was grown on the pretreated Si substrate. The difference in the morphology on the topside (RMS roughness: 3.3 nm) vs. the underside (RMS roughness: 0.3 nm) of the film is expected and is due to the columnar growth morphology observed in CVD-diamond films grown with H-rich gas chemistries [17]. The surface morphology on the underside (nucleation side) is remarkably smooth and uniform, consistent with an extremely high initial film nucleation density. Attempts to calculate the nucleation density from peaks identified in the AFM image using the software code mentioned above were unsuccessful due to the extremely smooth nature of the surface morphology. The actual nucleation density could therefore be far higher than 10^{12} nuclei/cm^2. This is in striking contrast with other nucleation methods, where the nucleation side often displays morphologies with crevices between coalescing grain colonies as observed in earlier studies [9,29].

To further investigate the diamond phase purity and the nature of carbon bonding on the top and undersides of the NCD film, we examined the free-standing NCD membranes with X-PEEM imaging (i.e. with spatially resolved XANES spectroscopy). Visible light microscopy revealed that, serendipitously, some portions of the membrane had partially folded over onto itself, so that regions of both the top and undersides were facing up. This enabled us to access both sides simultaneously, as shown in the optical micrograph of Fig. 4(a), taken in differential interference contrast mode. The darker region in the image is the topside, and the brighter region is the underside. The contrast occurs because the topside is rough and scatters light in multiple directions, thus appearing darker, while the underside is smooth and is more reflective at normal incidence. We verified the identification of the top and undersides by obtaining AFM images from each region since, as described above, the topography of the two sides are readily distinguished.

Fig. 4(b) shows the X-PEEM image of the same region shown in Fig. 4(a), taken at 285 eV. Bright corresponds to lower intensity in this image, so the contrast immediately suggests a heightened sp^2 content of the underside compared to the topside. The corresponding XANES spectra from the topside and underside are shown in Fig. 4(c). Both spectra show typical features of the phase-pure diamond surface with some minute differences in the top and undersides. For better comparison, the

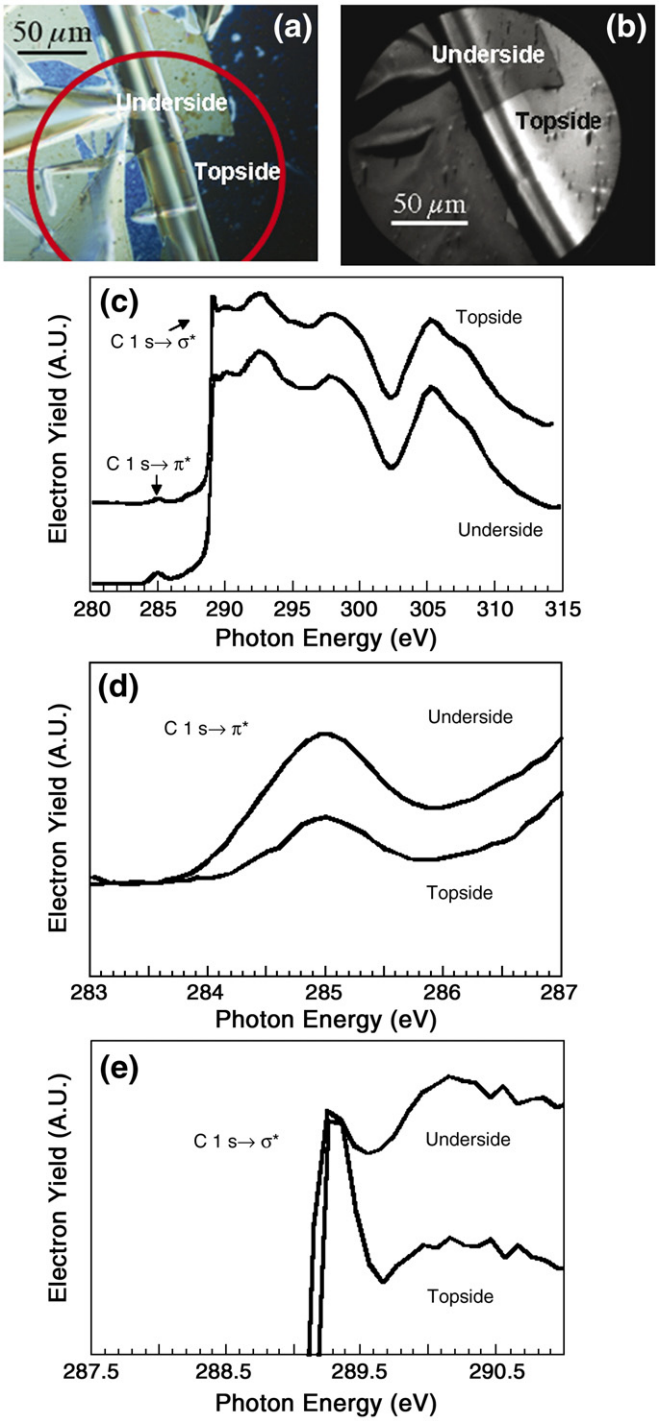

Fig. 4. (a) Visible light microscopy (VLM) image, obtained with differential interference contrast (DIC) of the free-standing 60 nm-thick NCD film, transferred onto a Si wafer. After this manual transfer, the film is partly folded, exposing both the topside and the underside film surfaces. The top and undersides appear dark and light, respectively. (b) X-PEEM image of the same area taken at 285 eV. (c) The XANES spectra acquired from the top and undersides of the 60 nm-thick NCD film respectively. Comparison of C1s→π* regions and C1s→σ* regions from the same spectra is shown in (d) and (e) respectively.

C1s→π* region and C1s→σ* regions from the top and undersides are plotted in a separate graph shown in Fig. 4(d) and (e) respectively. The C1s→π* peak at 285 eV is more prominent on the underside, and the diamond exciton (C1s→σ*) at 289.3 eV (indication of crystalline diamond bonding) on the underside is not as sharp on the topside. These observations demonstrate a slightly higher percentage of sp^2 bonding on the underside, but overall an overwhelmingly diamond character to the film on both sides. Analysis of 40 regions, a few micrometers in size in the field of view (FOV) from the PEEM image shown here, were consistent with this observation.

We quantified the sp^2 fraction for the top and underside surfaces using the following formula:

$$f_{sp^2} = \frac{I^{\pi^*}_{sam} I_{ref}(\Delta E)}{I^{\pi^*}_{ref} I_{sam}(\Delta E)'}$$

where $I^{\pi^*}_{sam}$ and $I^{\pi^*}_{ref}$ are the areas under the π* peak (285 eV) of the 60 nm NCD film and a reference sample of highly oriented pyrolytic graphite (HOPG) respectively, and $I_{sam}(\Delta E)$ and $I_{ref}(\Delta E)'$ are the areas calculated under the remainder of each spectrum (from 288.6 eV to 315 eV), which is the signal that arises from the sp^3-bonded carbon in each case. This calculation yielded a total sp^2 fraction to be 0.7%±0.09% (i.e. 99.3% sp^3) for the topside surface and 1.8%±0.15% (i.e. 98.2% sp^3) for the underside surface. This clearly shows the nearly perfect phase-pure nature of the topside surface of the NCD film. The remaining 0.7% on the growth surface may be due to grain boundaries, and adventitious carbon that deposits during etching and handling in air before the measurement. The slightly higher percentage of sp^2-bonded carbon on the underside surface is likely due to the amorphous hydrogenated carbon remaining from the plasma pretreatment process applied to the silicon substrate, which is not expected to be removed by our silicon etching procedure. In a previous study of ultrananocrystalline diamond (UNCD) films deposited on substrates exposed to the ultrasonic nucleation process, a significantly higher percentage of sp^2-bonded carbon was observed at the underside [9]. Addition of a small (5%) amount of H_2 during growth successfully etches away the sp^2-bonded carbon at the underside. However, this also etches the diamond nuclei, thereby reducing the initial nucleation density and increasing the grain size [30]. We suggest that the amount of sp^2-bonded carbon observed on the underside surface is a direct indication of the initial nucleation density and thus depends upon the nature of the nucleation pretreatment and seeding method used. Higher nucleation densities reduce the occurrences of crevices between neighboring coalescing grain colonies, and therefore reduce the formation of sp^2-bonded carbon in these crevices. Also, a reduced rate of diamond nucleation likely leads to an increased overall amount of non-diamond carbon deposition during the initial stage of growth. These issues are the subject of ongoing studies [31].

In conclusion, we have shown that the modified NNP process allows for the deposition of nearly phase-pure (>99% sp^3 bonding), ultra-thin (60 nm), ultrasmooth (3.3 nm RMS

over a 1 μm^2 area), continuous NCD films on Si. Detailed characterization of the nucleation process at each step revealed for the first time that the first plasma pretreatment step forms SiC along with a layer of ultra-thin, hydrogrenated, amorphous carbon on the substrate. The ultrasonication of nanodiamond seeds in the second step uniformly and densely spreads nanodiamond seed particles on this surface. This enables an extremely high nucleation density and minimizes precipitation of sp^2-bonded carbon during subsequent NCD growth. The underside of the film is much smoother (RMS roughness: 0.3 nm) than the topside (RMS roughness: 3.3 nm), and has only a slightly higher sp^2 content (1.8%) compared with the topside of the film (0.7%). This will help ensure that the attractive chemical, mechanical, and tribological properties of NCD are largely preserved on this etched underside. This is extremely attractive for MEMS/NEMS applications, where mechanical and tribological contacts between surfaces exposed by sacrificial etching of intermediate layers are common in many designs. The smoothness and compositional uniformity may also increase the fracture resistance and reduce mechanical dissipation.

Acknowledgements

We gratefully acknowledge Dr. John Carlisle from Argonne National Laboratory for his useful discussion regarding XANES spectra. We thank C. Bora for assistance with the peak analysis software. The X-PEEM experiments were performed at the UW Synchrotron Radiation Center (supported by NSF grant DMR 0084402) using the SPHINX microscope (Spectromicroscope for the PHotoelectron Imaging of Nanostructures with X-rays). RWC and PUPAG acknowledge the support from the Air Force Office of Scientific Research (AFOSR) grant # FA9550-05-1-0204. JEB acknowledges the support from the Office of Naval Research/Naval Research Laboratory.

References

[1] J. Philip, P. Hess, T. Feygelson, J.E. Butler, S. Chattopadhyay, K.H. Chen, L.C. Chen, J. Appl. Phys. 93 (2003) 2164.
[2] H.D. Espinosa, B. Peng, B.C. Prorok, N. Moldovan, O. Auciello, J.A. Carlisle, D.M. Gruen, D.C. Mancini, J. Appl. Phys. 94 (2003) 6076.
[3] T.H. Metcalf, X. Liu, B.H. Houston, J.W. Baldwin, J.E. Butler, T. Feygelson, Appl. Phys. Lett. 86 (2005) 81910.
[4] J.C. Arnault, L. Demuynck, C. Speisser, F. Le Normand, Eur. Phys. J., B Cond. Matter Phys. 11 (2) (1999) 327.
[5] E. Anger, A. Gicquel, Z.Z. Wang, M.F. Ravet, Diamond Relat. Mater. 4 (1995) 759.
[6] H.-W. Ko, C.K. Chen, C.-H.J. Liu, Diamond Relat. Mater. 5 (1996) 861.
[7] S. Pecoraro, J.C. Arnault, J. Werckmann, Diamond Relat. Mater. 14 (2005) 137.
[8] B.R. Stoner, G.H.M. Ma, S.D. Wolter, J.T. Glass, Phys. Rev., B 45 (1992) 11067.
[9] A. Sumant, D.S. Grierson, J.E. Gerbi, J. Birrell, U.D. Lanke, O. Auciello, J. Carlisle, R.W. Carpick, Adv. Mater. 17 (2005) 1039.
[10] S. Rotter, in: M. Yoshikawa, Y. Koga, Y. Tzeng, P. Klages, K. Miyoshi (Eds.), Proceedings of the Applied Diamond Conference/Frontier Carbon Technologies—ADC/FCT '99, 1999, p. 25, MYU, K.K, Tokyo, 1999.
[11] L. Sekaric, J.M. Parpia, H.G. Craighead, T. Feygelson, B.H. Houston, J.E. Butler, Appl. Phys. Lett. 81 (2002) 4455.
[12] V.Y. Dolmatov, Russ. Chem. Rev. 70 (2001) 607.
[13] B.H. Frazer, B. Gilbert, B.R. Sonderegger, G. De Stasio, Surf. Sci. 537 (2003) 161.
[14] B.H. Frazer, M. Girasole, L.M. Wiese, T. Franz, G.D. Stasio, Ultramicroscopy 99 (2004) 87.
[15] J.K. Simons, R.V. Duevel, S.P. Frigo, J.W. Taylor, R.A. Rosenberg, J. Appl. Phys. 76 (1994) 5481.
[16] D.N. Belton, S.J. Harris, S.J. Schmieg, A.M. Weiner, T.A. Perry, Appl. Phys. Letts. 54 (1989) 416.
[17] R.F. Davis, Edited by R. F. Davis, Noyes Publication, Park Ridge, New Jersey, USA. (1992).
[18] O.A. Shenderova, I. Petrov, J. Walsh, V. Grichko, V. Grishko, T. Tyler, G. Cunningham, ICNDST-ADC Conference, May 15–18, 2006, Raleigh, NC, USA, 2006.
[19] A. Scholl, Y. Zou, M. Jung, T. Schmidt, R. Fink, E. Umbach, J. Chem. Phys. 121 (2004) 10260.
[20] M.M. Garcia, I. Jimenez, O. Sanchez, C. Gomez-Aleixandre, L. Vazquez, Phys. Rev., B 61 (2000) 10383.
[21] J. Steeds, M.A., T. Murimura, J.E. Butler, Personal communication.
[22] J. Stöhr, NEXAFS Spectroscopy, Springer-Verlag, Berlin, Heidelberg, 1992.
[23] R. Gago, M. Vinnichenko, H.U. Jager, A.Y. Belov, I. Jimenez, N. Huang, H. Sun, M.F. Maitz, Phys. Rev., B 72 (2005) 14120.
[24] K. Kanda, T. Kitagawa, Y. Shimizugawa, Y. Haruyama, S. Matsui, M. Terasawa, H. Tsubakino, I. Yamada, T. Gejo, M. Kamada, Jpn. J. Appl. Phys. 41 (2002) 4295.
[25] J.F. Morar, F.J. Himpsel, G. Hollinger, J.L. Jordan, G. Hughes, F.R. McFeely, Phys. Rev., B 33 (1986) 1340.
[26] J.F. Morar, F.J. Himpsel, G. Hollinger, G. Hughes, J.L. Jordan, Phys. Rev. Lett. 54 (1985) 1960.
[27] J.Y. Raty, G. Galli, C. Bostedt, T.W. van Buuren, L.J. Terminello, Phys. Rev. Lett. 90 (2004) 37401.
[28] C.K. Bora, E.E. Flater, M.D. Street, J.M. Redmond, M.J. Starr, R.W. Carpick, M.E. Plesha, Tribol. Lett. 19 (2005) 37.
[29] S.H. Seo, W.C. Shin, J.S. Park, Thin Solid Films 416 (2002) 190.
[30] S. Jiao, A. Sumant, M.A. Kirk, D.M. Gruen, A.R. Krauss, O. Auciello, J. Appl. Phys. 90 (2001) 118.
[31] A.V. Sumant, D.S. Grierson, J. Gerbi, J. Birrell, J. Carlisle, O. Auciello, R.W. Carpick, in preparation.